BRILLIANCE AND FLUX REDUCTION IN IMPERFECT INCLINED CRYSTALS*

W. K. Lee, R. C. Blasdell, P. B. Fernandez, A. T. Macrander, and D. M. Mills
Experimental Facilities Division, Advanced Photon Source,
Argonne National Laboratory, Argonne, IL 60439

January 1996

Presented at the SRI '95 APS X-ray Centennial Symposium/Seventh Users Meeting for the APS, Argonne, IL, October 16-20, 1995; to be published in the proceedings as a peer-reviewed volume of the *Review of Scientific Instruments* in CD-ROM format.

*This work supported by the U.S. Department of Energy, Basic Energy Sciences-Materials Sciences, under contract #W-31-109-ENG-38.

Brilliance and Flux Reduction in Imperfect Inclined Crystals

W. K. Lee, R. C. Blasdell, P. B. Fernandez, A. T. Macrander and D. M. Mills
Experimental Facilities Division, Advanced Photon Source, Argonne National Laboratory, Argonne, Illinois 60439

(Presented on 19 Oct 1995)

The inclined crystal geometry has been suggested as a method of reducing the surface absorbed power density of high-heat-load monochromators for third-generation synchrotron radiation sources. Computer simulations have shown that if the crystals are perfectly aligned and have no strains then the diffraction properties of a pair of inclined crystals are very similar to a pair of conventional flat crystals with only subtle effects differentiating the two configurations. However, if the crystals are strained, these subtle differences in the behavior of inclined crystals can result in large beam divergences causing brilliance and flux losses. In this manuscript we elaborate on these issues and estimate potential brilliance and flux losses from strained inclined crystals at the APS.

I. INTRODUCTION

The inclined crystal geometry, as shown schematically in Figure 1, was originally suggested [1,2] as a method of reducing the surface-absorbed power density of high-heat-load x-ray monochromators for third-generation synchrotron sources. Computer simulations [3] have shown that if the crystals are perfectly aligned and have no strains (thermal or mechanical), then the diffraction properties of an inclined, double-crystal monochromator (DCM) should be fairly similar to that of conventional flat crystals; that is, the asymmetry parameter, $b = \mathbf{k}_{inc}.\mathbf{n}/\mathbf{k}_{out}.\mathbf{n} \approx -1$ for the inclined crystal. Several synchrotron tests of the inclined geometry have proven that it is indeed an effective method for reducing the thermal strains in single-crystal high-heat-load x-ray monochromators [4,5].

Ray-tracing results [3,6,7], however, have revealed that, under certain conditions, the subtle differences between the inclined geometry and the conventional flat geometry may be significant. In particular, small thermal or mechanical strains can induce a large transverse beam divergence causing large brilliance and flux losses. The object of this paper is to elaborate on these issues and to remind potential users of the possible pitfalls of the inclined crystal geometry.

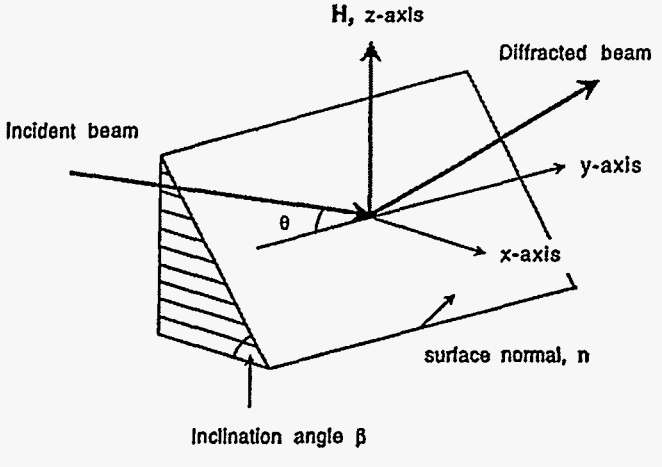

Fig. 1. Schematic of the inclined crystal geometry

II. THEORETICAL DISCUSSION

To understand the cause of these pitfalls, it is useful to review the essential points of the inclined-crystal geometry. It is assumed here that the reader has some understanding of dynamical diffraction theory [8-11]. This discussion will be based on the approach of Batterman and Cole [10]. With exception of the experimental results, the discussion will use the reference axes as shown in Figure 1.

Figure 2 shows a familiar dispersion surface. For conventional symmetric and asymmetric reflections, a 2-D picture of the dispersion and Laue spheres [11] is sufficient; i.e., the reciprocal lattice vector, **H**, the crystal surface normal, **n**, and ALL the wave vectors (incident and reflected, inside and outside the crystal) lie in the same plane (and thus can be drawn on a piece of paper). The waves inside the crystal and the external exit wave, $\mathbf{k}_{out}$, are determined by the so-called tie points, which are the intersection of the crystal normal, **n**, to the dispersion surfaces (for the internal waves) and to the "exit Laue sphere". (The "exit Laue sphere" and "entrance Laue sphere" are defined as spheres of radius $k = |\mathbf{k}_{inc}| = |\mathbf{k}_{out}|$ centered at **H** and **O** respectively. **O** is the origin of the reciprocal lattice. For later reference, points A and C in Figure 2 shall be referred to as "entrance" and "exit" points.) However, in the case of the inclined geometry, the normal to the crystal surface, **n**, lies out of the plane spanned by the incoming wave vector, $\mathbf{k}_{inc}$ and **H** (YZ plane in Figure 2). Thus, the tie points on the dispersion surfaces (which correspond to the internal wave vectors) and the exit point (point C in Figures 2 and 3) will not lie in the YZ plane. Figure 3 shows a 3-D version of the dispersion surfaces. The important thing to note is that the exit beam, $\mathbf{k}_{out}$, is now out of the YZ plane. We refer to this out-of-plane effect on the diffracted beam as a "rho-kick" or ρ_{refl}. It is easy to see that, for a particular inclination angle (or **n**), the amount of rho-kick is dependent on the incidence angle. As the incidence angle changes, the entrance point moves along the surface of the entrance Laue sphere, causing the exit tie

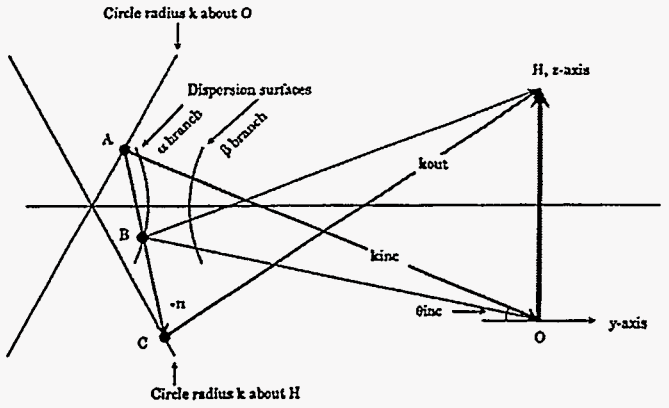

Fig. 2. A typical "conventional" dispersion surface diagram for the general case where n is in the plane spanned by H and k_{inc}, but not necessarily parallel to H. For clarity, only the σ polarization surfaces are shown. For the case drawn here, there is only one tie-point, B. $k = |k_{inc}| = |k_{out}|$. AO is the (external) incident wave vector, k_{inc}. B is the intersection of the α dispersion surface with a vector through A ("entrance point"), parallel to the crystal normal, n. Similarly, C ("exit point") is the intersection of a circle of radius k about H with a vector through A, parallel to the crystal normal, n. BO and BH are the internal diffracted beams, $K_O^{\alpha\sigma}$ and $K_H^{\alpha\sigma}$. Note that $|K| < k$ due to the index of refraction. CH is the external diffracted beam.

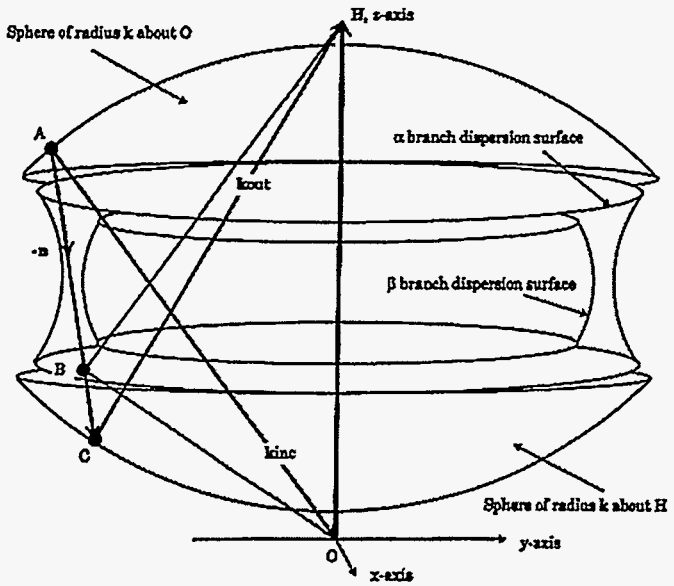

Fig. 3. A 3-D version of the dispersion surface diagram. As in Figure 2, only the σ polarization surfaces are shown. As before, AO is the external incident wave vector, k_{in}. B is the intersection of the α branch of the dispersion surface with a vector through A, parallel to the crystal normal, n. Similarly, C is the intersection of a sphere of radius k about H with a vector through A, parallel to the crystal normal, n. BO and BH are the internal diffracted beams. A, O, and H all lie in the YZ plane (plane of the paper). But now, B and C lie out of the YZ plane. Thus, the external diffracted beam, CH, no longer lies in the YZ plane. Note that the normal, as drawn here depicts an asymmetric inclined (or rotated inclined) geometry. For a symmetric inclined crystal geometry, the normal n, would lie in the ZX plane. In other words, if we had drawn the normal for the symmetric case here, it would be parallel to OH (the projection of n would be parallel to H).

point to move along the exit Laue sphere. By simple geometry, one can easily map out the ρ_{refl} (rho-kick) dependence on the incidence angle θ_{inc}. Figure 4 shows the definition of the rho-kick angle, ρ_{refl}, and several other angles of relevance to this discussion. The definition of ρ_{refl} is similar to that in reference [3]. $\delta\theta_{xml}$ is defined as the angle between k_{out} and k_{out} projected onto the YZ plane. That is,

$$\delta\theta_{xml} = \sin^{-1}\left(\frac{k_{out} \cdot \hat{x}}{|k_{out}|}\right). \qquad (1)$$

Figure 5, which is the crux of this paper, shows, for Si(111) crystals of various inclination angles, the rho-kick dependence on $\theta_{inc} - \theta_{Bragg}$ for a single reflection. (θ_{inc} is the incidence angle, and θ_{Bragg} is the kinematic Bragg angle.) The slopes, which depend on the inclination angle, are almost linear and are almost independent of energy. For an 85° inclined crystal, the slope of the line is about 22, while that for a 78° inclined crystal is about 9.2. Figure 6 shows a plot of θ_{inc} vs θ_{refl} for an 85° inclined Si(111) crystal diffracting at 13.84 keV. We see that, although $\theta_{inc} \neq \theta_{refl}$, the difference is very small. Because ρ_{refl} varies almost linearly with $\theta_{inc} - \theta_{Bragg}$, and $\theta_{inc} \approx \theta_{refl}$, we can also treat Figure 5 as a plot of the rho-kick from a double-inclined-crystal monochromator (+/- geometry) versus the θ misorientation angle between the two crystals, $\Delta\theta = \theta 1_{out} - \theta 2_{inc} \approx \theta 1_{inc} - \theta 2_{inc}$. In other words:

$$\rho 2_{refl} \cong \frac{d\rho 1_{refl}}{d\theta 1_{inc}} \cdot \Delta\theta \qquad (2)$$

For a set of perfect inclined crystals in the parallel (+/-) geometry, the rho-kick does not present a problem because, by reversibility, the second crystal of the DCM will add its own rho-kick, which exactly cancels out the rho-kick from the first crystal. The doubly diffracted beam will thus still be parallel to the incoming beam, k_{inc}, although there will be a

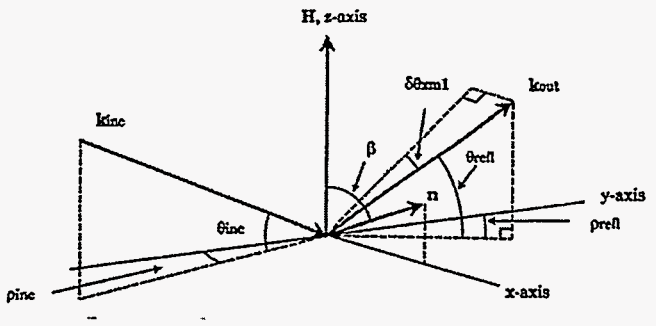

Fig. 4. Definition of some relevant angles in the inclined geometry. The ρ angles are defined as the angle between the y-axis and the appropriate k vector projected onto the XY (or Bragg) plane. β is the inclination angle. The horizontal divergence of the beam is characterized by the angle $\delta\theta_{xml}$, which is the actual 'out-of-plane' angle. Notice that $\delta\theta_{xml} < \rho_{refl}$; the difference is more pronounced at higher Bragg angles. ($\delta\theta_{xml}/\rho_{refl}$) ≈ 0.995, 0.97, and 0.87 for 20 keV, 8 keV, and 4 keV, respectively. The ratio is independant of β.

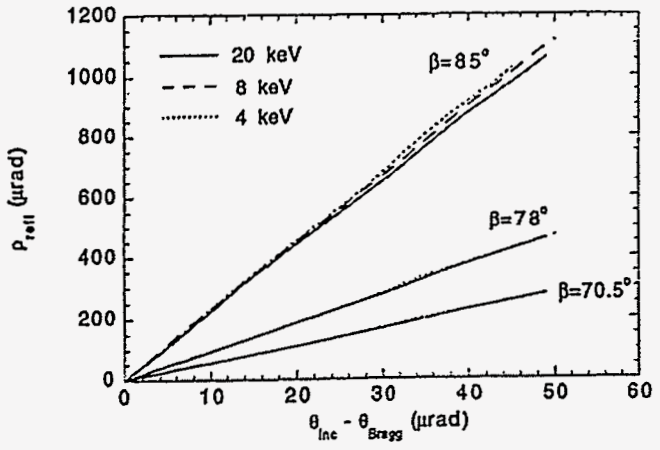

Fig. 5. Plot of ρ_{refl} versus $\theta_{inc} - \theta_{Bragg}$ for Si(111) single reflection for various inclination angles and energies. The incoming beam is highly collimated with $\rho_{inc} = 0$. At the kinematic Bragg angle, θ_{Bragg}, $\rho_{refl} = 0$. As explained in the text, this can also be viewed as a plot of ρ_{refl} versus $\Delta\theta$ misalignment between a (+/-) pair of inclined crystals in a DCM.

very slight transverse offset. Due to the extremely high slopes shown in Figure 5, the problem occurs when there is a slight difference between $\theta 1_{refl}$ and $\theta 2_{inc}$. This may occur, for example, if one crystal has fabrication/mounting/thermal-induced strains. Then, the rho-kick from the second reflection will not exactly cancel the rho-kick from the first reflection. Compared to the flat crystal geometry, the effect of these strains are highly amplified (by the values of the slopes in Figure 5) in the inclined crystal geometry. For example, in the case of an 85° inclined DCM, the slope (Figure 5) is about 22. Thus, a θ misalignment of 1 μrad between the two crystals would induce a 22 μrad horizontal divergence in the monochromatic beam.

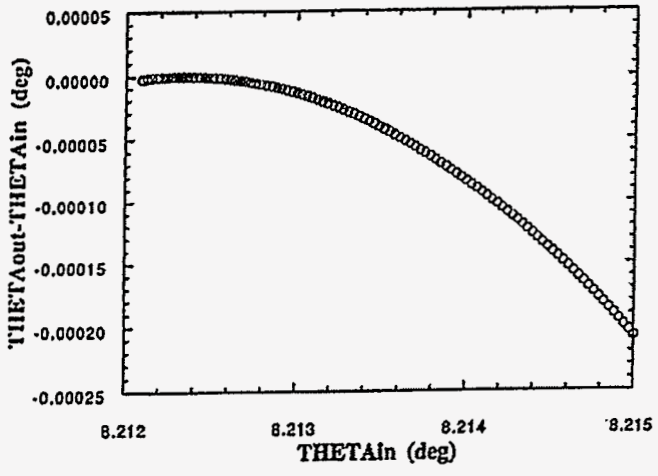

Fig. 6. Plot of $\theta_{refl} - \theta_{inc}$ versus θ_{inc} for an 85° inclined Si(111) crystal reflecting at 13.84 keV [3]. Although $\theta_{refl} \neq \theta_{inc}$, the difference is small.

III. EXPERIMENTAL RESULTS

Several in-house measurements have been made to verify the above simulations. The measurements were performed with a Spellman x-ray generator with a copper anode, operating at 50 kV x 40 mA. A pair of 2 mm x 2 mm slits were placed at the exit window of the Spellman generator to cut down background scattering. A ~8.5-m-long evacuated beam pipe transported the beam to the experimental hutch. A pair of 1 mm x 1 mm slits were placed inside the hutch, near the first crystal. The distance from these defining slits to the source is about 9 m. The measurements were performed with the first crystal scattering horizontally (opposite to the synchrotron and Figure 1) and the second crystal scattering vertically. Rocking curves (RCs) were obtained by rotating the second crystal. (The term "rocking-curve" is used very loosely here as these measurements are very different from the conventional double-crystal rocking curves.) The rocking curves should therefore be sensitive to any rho-kick from the first crystal. Figure 7 shows a schematic of the experimental setup. Note, however, referring to Figure 4, that it is actually $\delta\theta_{xm1}$ that gets convoluted into the RC width for the second (analyzer) crystal and not ρ_{refl}. However, for the 8-keV case, the difference between $\delta\theta_{xm1}$ and ρ_{refl} is very small (~3%, see later section). The same second crystal (flat Si(111)) was used in all the measurements. All reflections were from the Si(111) planes, and the energy was 8.04778 keV ($CuK_{\alpha 1}$ line). The width of the rocking curve is therefore a function of the vertical divergence of the incoming beam, the energy width of the $CuK_{\alpha 1}$ line, and the Darwin width. Because the horizontal divergence of the beam incident on the first crystal exceeds the Darwin width, the vertical divergence of the beam off the first crystal has a contribution equal to the Darwin width times the magnification factor due to the rho-kick effect. The measured RCs are generally Gaussian in shape. The results are shown in Table I.

While detailed simulations of the experiments are still being carried out, some simple interpretations can be made. As mentioned above, the RC widths should be a function of the vertical divergence off the first crystal, the energy width of the $CuK_{\alpha 1}$ line, and the Darwin width. Every photon reflected by the first crystal must have hit the first crystal at the right angle (Bragg angle plus the small refractive index correction) to within half the Darwin width. Therefore, for the inclined-crystal case, the range of rho-kick from first

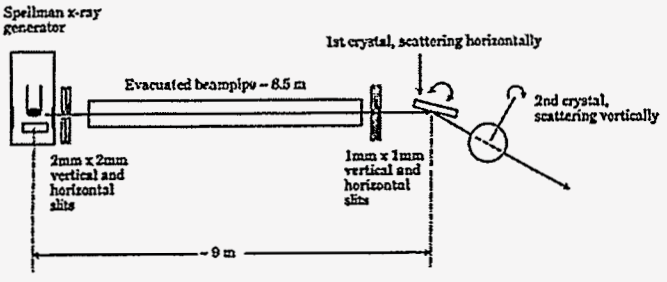

Fig. 7. Experimental setup used to verify the ρ_{refl} simulations. For ease of drawing and clarity, the flat crystal case is shown.

Table I: RC width comparisons between flat and inclined first crystal. Setup as shown in Figure 7.

	Flat first crystal - flat second crystal	85° inclined first crystal - flat second crystal
Measured FWHM	37.6" +/- 2"	157" +/- 6"

crystal should be about 22 times (slope of the line in Figure 5) the Darwin width (6.8") = 150". (The actual value of the ρ_{refl} should vary from about 64" to about 214". But because we have an arbitrary zero in the rotation, the RC measurement only records the width of the divergence.) If we assume that the rho-kick adds in quadrature to the measured value for the flat-flat case, we see that the RC for the good inclined crystal should be $\sqrt{37.6^2+150^2}=155"$. The measured value was 157". This first set of measurements clearly supports the simulations shown in Figure 5.

For the second set of measurements, a channel-cut first crystal was used, scattering in the horizontal plane. The flat second-crystal analyzer remained the same as for the previous measurements, scattering in the vertical plane. These measurements would better simulate an actual inclined DCM. According to the simulations, if the channel-cut crystal is totally strain free, then we should not see any increase in the vertical beam divergence after the channel-cut crystal. The rho-kick from the second channel-cut reflection would exactly undo the rho-kick from the first channel-cut reflection. On the other hand, if the channel-cut crystal is strained, we should see an increase in the vertical divergence after the channel-cut crystal. The increase in vertical divergence depends on the difference between the angle at which the photon leaves the first reflecting surface, $\theta 1_{out}$, and the angle at which the photon hits the second reflecting surface, $\theta 2_{inc}$. This may occur if the crystal is strained. Using Figure 5, we can predict the amount of rho-kick from an inclined DCM if we know the relative strain between the two crystals.

The channel-cut crystal was fabricated such that it can be used as a normal flat-flat Si(111) channel-cut crystal or as a 70.5° inclined-inclined channel-cut crystal. Measurements were made with the channel-cut crystal in both the flat and the inclined geometries for comparison. As before, rocking curves were measured by rotating the second flat analyzer crystal, scattering vertically. The results of the triple bounce RC (flat horizontal - flat horizontal - flat vertical on one hand, and inclined horizontal - inclined horizontal - flat vertical on the other hand) are shown in Table II. The slope of the rho-kick, ρ_{refl} vs $\theta_{inc} - \theta_{Bragg}$ plot for the case of a 70.5° inclined crystal, is about 5.5. (As before, although we are actually sensitive to $\delta\theta_{xml}$ and not ρ_{refl}, the difference between the two is very small at this Bragg angle.)

Again, if we assume that the rho-kick adds in quadrature to the RC width, we see that the inclined channel-cut case has an increased vertical divergence of about $\sqrt{43^2-39^2}=18"$. If we assume that this is all due to the rho-kick effect (see discussion below), this suggests that there is 18/5.5 = 3.3" strain in the channel-cut crystal. This is slightly higher than the measured strain of 2", a value we measured using MoK_α radiation in the flat Si(333) geometry. The ratio (3.3/2 = 1.65 times) can be explained as follows: (1) the strain measurements were performed at a much higher energy (17.5 keV) in the flat Si(333) geometry, (2) the beam footprint on the crystal is larger in the inclined case, and thus the strain as seen by the beam may be larger, (3) the beam is more grazing in the inclined case and is probably more sensitive to surface roughness. For the same reasons (2&3), the increased vertical divergence of 18" should be considered only as an upper limit to the possible rho-kick effect; i.e., the effect of the rho-kick phenomena is very likely less than 18". However, until detailed simulations are performed, this is a good starting point.

Because the difference between the inclined and flat measurements was quite small in the above case, we decided to "rough up" (with 240 grit SiC) the first reflecting surface of the channel-cut to get a bigger effect. The measured strain using MoK_α radiation in the flat Si(333) geometry was 13" for the roughened crystal. Comparing the inclined and flat cases, we see that there is an increase of $\sqrt{141^2-69^2}=123"$ in the vertical divergence of the beam from the inclined channel-cut. As before, if we assume that this is entirely due to the rho-kick effect, we obtain a strain field in the crystal of 123/5.5 = 22.4". The ratio of this number to the measured strain is 22.4/13 = 1.72, which compares quite well with the similar ratio of 1.65 in the previous measurement.

Finally, in order to confirm that, without strains, the inclined and flat cases should be identical, we etched the channel-cut crystal thoroughly (removed ~ 0.006" surface material) and checked with MoK_α radiation in the flat Si(333) geometry that it is indeed strain free. Then, we repeated the above measurements. In this case, we find that there is no difference in the RC width between the flat channel-cut crystal case and inclined channel-cut-crystal case, as expected.

These measurements clearly support the rho-kick effect simulations as shown in Figure 5.

IV. BRILLIANCE AND FLUX LOSS ESTIMATES

In order to estimate the brilliance and flux losses due to the rho-kick effect described above, a phase space discussion of the source and the effect of the crystal on the phase space is useful. At the APS, the radiation characteristics are dominated by the emittance of the stored positron beam. At energies above 5 keV, the contributions to the beam size and divergence of the x-ray photon beam arising from diffraction limitations can be neglected; i.e., only the particle beam contributions need to be considered. Under these assumptions, the product of the source photon emittances of the APS undulator A can be written as [12]:

$$\begin{aligned}\zeta &= \varepsilon_x \cdot \varepsilon_y \\ &= \Sigma_x\Sigma_{x'} \cdot \Sigma_y\Sigma_{y'} \\ &= (325\text{ mm})(23\text{ mrad}) \cdot (86\text{ mm})(9\text{ mrad}) \quad (1\ \sigma\text{ values}) .\end{aligned} \tag{3}$$

Table II: RC width comparisons with a channel cut first crystal in the flat and inclined orientations. Setup is as shown in Figure 7.

Measured FWHM	Flat channel-cut first crystal - flat second crystal	70.5° inclined channel-cut first crystal - flat second crystal
Original channel-cut	39 +/- 2"	43 +/- 2"
First reflection surface roughened with 240 grit	69 +/- 4"	141 +/- 9"
After a long acid etch	40 +/- 2"	40 +/- 2"

Here ε_x and ε_y are the horizontal and vertical phase spaces emittances, Σ_x and Σ_y are the horizontal and vertical source photon beam sizes, and $\Sigma_{x'}$ and $\Sigma_{y'}$ are the horizontal and vertical source photon beam divergences. Figure 8 shows schematically, for a particular wavelength, the vertical phase space at the source with the major axes along the y and y' directions. By the time the beam reaches the nominal position of the first crystal monochromator (Figure 8(b)) the ellipse is significantly stretched out in the y axis. The long major axis of the ellipse is now inclined with a slope

$$m_v = \frac{1}{d_{m1}}, \tag{4}$$

where d_{m1} is the distance from the source to the center of the crystal. The width of the ellipse at a given value of y' is still characterized by Σ_y, but now the total width of the ellipse is given by

$$\Delta y = \Sigma_{y'} \cdot d_{m1} . \tag{5}$$

The total height of the ellipse (in y') is still characterized by $\Sigma_{y'}$, but now the width of the divergence distribution at a given value of y is given by

$$\Delta y'_c = \frac{\Sigma_y}{d_{m1}} . \tag{6}$$

This is the divergence arising from the source size, and it is this quantity that is of use in a discussion about the preservation of brilliance through a crystal. For the APS undulator A with the first crystal at d_{m1} = 30 m, one finds that (1 σ values)

$$\Delta y'_c = 86\ \mu m/30\ m = 2.9\ \mu rad$$

$$\Delta x'_c = 325\ \mu m/30\ m = 10.8\ \mu rad ,$$

where $\Delta x'_c$ is the equivalent quantity for the horizontal phase space.

Ignoring reflectivity losses, for a strain-free symmetric crystal whose Darwin acceptance width is larger than $\Sigma_{y'}$ and whose physical size is larger than Δy, the phase space immediately after the crystal looks the same as the phase space immediately before the crystal. (If the Darwin acceptance width is smaller than $\Sigma_{y'}$ and/or the physical size of the crystal is smaller than Δy, then the phase space ellipse after the crystal will be limited in the y' axis by the Darwin width and in the y axis by the physical size of the crystal.) If a strain field exists in the crystal that has a distribution of slopes at each meridinal (vertical) point on the crystal

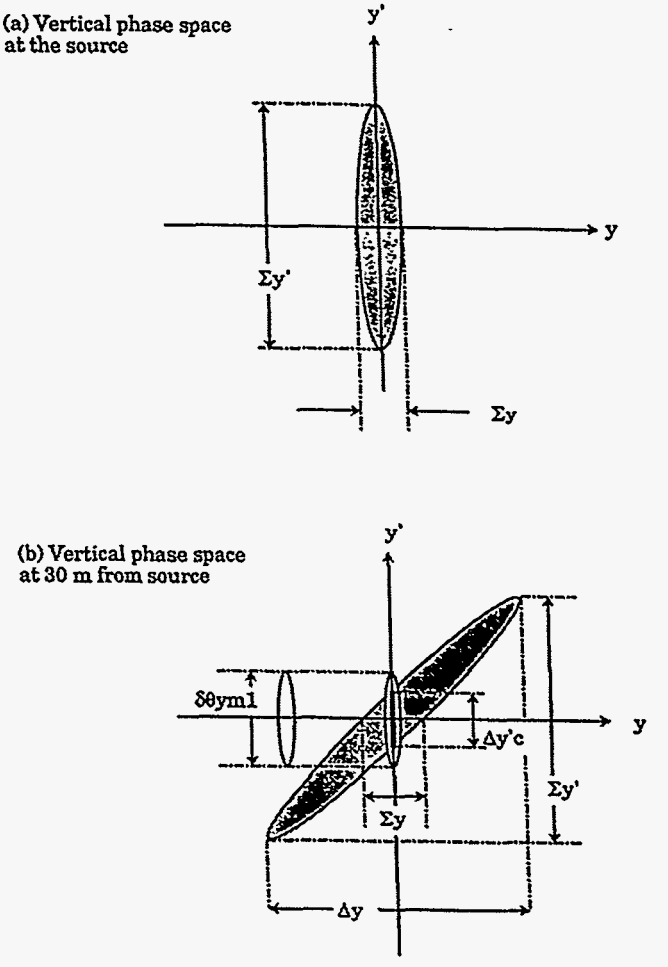

Fig. 8. Schematic drawing of the vertical phase space (shaded ellipse) of the undulator A beam at the source (a) and at the nominal monochromator first crystal position (b) 30 m from the source. Note that the ellipse is stretched in y as the beam diverges. The two open ellipses in (b) schematically show a "mosaic" broadening function, which, if convolved with the beam emittance at each value of y, would significantly increase the area of the ellipse (the emittance) and therefore decrease the brilliance of the reflected beam. Note that the width of this function $\delta\theta_{ym1}$ must be kept less than or equal to the quantity $\Delta y'_c$ in order that there be no significant brilliance loss. Also note that $\Delta y'_c \ll \Sigma_{y'}$, the source vertical divergence. A similar picture can be drawn for the horizontal phase space.

characterized by the quantity $\delta\theta_{yc1}$, a smearing of the vertical divergence of the reflected beam at each value of y by $\delta\theta_{ym1}$ (equal to 2 $\delta\theta_{yc1}$ for the symmetric case) is produced. Then in order for there to be no significant loss in beam emittance, the condition

$$\delta\theta_{ym1} \le \Delta y'_c = \frac{\Sigma_y}{d_{m1}} \tag{7}$$

must be satisfied. This is schematically represented in Figure 8(b), where the open ellipses (which represent the mosaic broadening function at two y-points) are shown slightly larger than $\delta\theta_{ym1}$ but much narrower than $\Sigma_{y'}$. Clearly, if this "mosaic" was present in the crystal, it would noticeably broaden the phase ellipse of the reflected beam.

Assuming that the quantitites add in quadrature and that reflectivity losses are negligible, one can estimate the vertical phase space emittance immediately downstream of the monochromator as

$$\varepsilon_{ym1} \cong \Delta y \cdot \sqrt{(\Delta y'_c)^2 + (\delta\theta_{ym1})^2} \tag{8}$$

$$= \Sigma_{y'} d_{m1} \cdot \sqrt{\left(\frac{\Sigma_y}{d_{m1}}\right)^2 + (\delta\theta_{ym1})^2}$$

$$= \sqrt{(\Sigma_y \cdot \Sigma_{y'})^2 + (\Delta y \cdot \delta\theta_{ym1})^2} \ .$$

A similar expression holds for the horizontal phase space. In general, if the total smearing of the reflected beam vertical divergence (averaged over x at each point y) is characterized by $\delta\theta_{ym1}$, and the total smearing of the reflected beam horizontal divergence (averaged over y at each point x) is characterized by $\delta\theta_{xm1}$, then the product of the reflected beam emittances is approximately

$$\zeta_{m1} \cong \sqrt{(\Sigma_x \cdot \Sigma_{x'})^2 + (\Delta x \cdot \delta\theta_{xm1})^2}$$

$$\times \sqrt{(\Sigma_y \cdot \Sigma_{y'})^2 + (\Delta y \cdot \delta\theta_{ym1})^2} \ . \tag{9}$$

The beam brilliance is inversely proportional to the product of the horizontal and vertical beam emittances. The brilliance loss, (B_{m1}/B_0), due to the strain field is then

$$\frac{B_{m1}}{B_0} \cong \frac{(\Sigma_x \cdot \Sigma_{x'}) \cdot (\Sigma_y \cdot \Sigma_{y'})}{\zeta_{m1}} \tag{10}$$

For a symmetric flat crystal with a randomly distributed slope error of the crystalline planes of $\delta\theta_{c1}$, the reflected beam (assuming diffracting in the vertical plane) will have increased vertical ($\delta\theta_{ym1}$) and horizontal ($\delta\theta_{xm1}$) divergences given by:

$$\delta\theta_{ym1} \approx 2\,\delta\theta_{c1} \tag{11}$$

$$\delta\theta_{xm1}(\text{flat crystal}) \approx \sin^{-1}\left(\frac{2\sin\theta\tan(\delta\theta_{c1})}{1+\tan^2(\delta\theta_{c1})}\right) . \tag{12}$$

(The above expression for $\delta\theta_{xm1}$ is equivalent to a tilt (or chi) misalignment.) For an inclined crystal, the rho-kick effect adds to the horizontal divergence, and, for the relatively small Bragg angles encountered here, the rho-kick effect will dominate.

Refering to Figure 4, it is perhaps useful to note the small difference between $\delta\theta_{xm1}$ and ρ_{refl}. In terms of k_{out} and the reference axes, $\hat{x}$, $\hat{y}$, and $\hat{z}$:

$$\rho_{refl} = \tan^{-1}\left(\frac{k_{out} \cdot \hat{x}}{k_{out} \cdot \hat{y}}\right) \tag{13}$$

$$\delta\theta_{xm1} = \sin^{-1}\left(\frac{k_{out} \cdot \hat{x}}{|k_{out}|}\right) . \tag{14}$$

The ratio $(\delta\theta_{xm1}/\rho_{refl}) \approx 0.995$, 0.97, and 0.87 for the Si(111) 20 keV, 8 keV, and 4 keV cases, respectively. The ratio is independent of β.

Based on our current estimates/measurements of fabrication and thermally induced strains, we can estimate the severity of the brilliance loss for gallium-cooled flat and inclined Si(111) crystals. With the current methods of crystal fabrication (particularly, the bonding process), the typical strain induced in the crystal is about 6 μrad (1 σ value) over the entire 4-inch diameter surface. For the thermal-induced strains, we base our estimates on the results of reference [13].

For the flat geometry case:

$$\delta\theta_{ym1} = 2\,\delta\theta_{c1}$$

$$\delta\theta_{xm1} \approx 0.5\,\delta\theta_{c1} \quad \text{for Bragg angle of } 14.2°.$$

For the 78° inclined geometry (8-keV) case:

$$\delta\theta_{ym1} = 2\,\delta\theta_{c1}$$

$$\delta\theta_{xm1} \approx 9.0\,\delta\theta_{c1}.$$

For the 85° inclined geometry (4-keV) case:

$$\delta\theta_{ym1} = 2\,\delta\theta_{c1}$$

$$\delta\theta_{xm1} \approx 19.7\,\delta\theta_{c1},$$

where, as described above, $\delta\theta_{c1}$ (fabrication) = 6 μrad, and $\delta\theta_{c1}$ (thermal) = 5.5 μrad for the 85° inclined, 4-keV case and 2.5 μrad for the 78° inclined, 8-keV case.

The effect of the various beam divergences on the beam brilliance for a flat crystal, a 78° inclined crystal (with the APS undulator A first harmonic of 8 keV), and an 85° inclined crystal (with the APS undulator A first harmonic of 4 keV) are shown in Table III. All crystals are Si(111), and

Table III: Brilliance loss, (B_{m1}/B_o), as defined in equation (10), for the case of flat and inclined geometry.

Crystal	Energy (keV)	Fab. strain (μrad)	Thermal strain (μrad)	Total strain (μrad)	B_{m1}/B_o (fab)	B_{m1}/B_o (thermal)	B_{m1}/B_o (total)
Flat		6			0.22		
78° incl.	8	6	2.5	6.5	0.045	0.22	0.04
85° incl.	4	6	5.5	8.1	0.021	0.025	0.01

Table IV: Flux loss, (F_{m1}/F_o), as defined by equation (17), for the case of flat and inclined geometry.

Crystal	Energy (keV)	Fab. strain (μrad)	Thermal strain (μrad)	Total strain (μrad)	F_{m1}/F_o (fab)	F_{m1}/F_o (thermal)	F_{m1}/F_o (total)
Flat		6			0.83		
78° incl.	8	6	2.5	6.5	0.54	0.87	0.50
85° incl.	4	6	5.5	8.1	0.30	0.33	0.21

the thermal results assume a 100-mA ring current. We assume that the total strain consists of the strains from the fabrication-induced and thermal-induced strains added in quadrature. The brilliance loss estimate for the thermal-induced and total strain, flat-crystal case is not given because there is no data for the expected thermal-induced strain for a flat crystal. (However, it has been calculated that, for a closed-gap situation, with a flat, gallium-cooled crystal oriented for 4-keV Si(111) reflection, the temperature on the crystal would approach its melting point!)

Thus, based on our present crystal cooling and fabrication capabilities, the brilliance loss estimates for both inclined crystal cases presented here would appear unacceptable. Comparing the brilliance loss due to the estimated fabrication-induced strains, one sees that a 78° inclined crystal would be 5 times while the 85° inclined crystal would be 10 times worse than the flat crystal. Taking the thermal strains into account, these estimates predict that for the 85° inclined case, the brilliance may be down by a factor of 100 compared to the incoming beam! It is true that the situation would improve somewhat with a lower inclination angle (slope of Figure 5 would decrease). However, unless a better cooling scheme is realized, the lower inclination angle would most likely result in a higher thermal-induced strain. Table III strongly suggests that if brilliance is of importance to the experimenter, and lower fabrication strains are not achieved, then the inclined crystal geometry would not be a good candidate for the high-heat-load monochromator. We note that these statements apply to the total (vertical x horizontal) brilliance. Users who are interested only in the vertical part should not be similarly concerned since the extra brilliance losses introduced by the inclined geometry are confined to the horizontal part of the of the overall brilliance.

For the user who is more interested in photon flux (photons/s/mm^2) rather than brilliance, it is useful to make similar flux comparisons between the flat and inclined crystal geometries. For the APS 1-ID beamline, the monochromator is at d_{m1} = 30 m from the source and the monochromatic hutch is at d' = 30 m from the monochromator (60 m from the source). Thus, the undistorted beam sizes, as given in equations (3 & 5) are:

$$\Delta y = \Sigma_{y'} \cdot (d_{m1} + d') = 9\ \mu\text{rad} \times 60\ \text{m} = 540\ \mu\text{m}$$

$$\Delta x = \Sigma_{x'} \cdot (d_{m1} + d') = 23\ \mu\text{rad} \times 60\ \text{m} = 1380\ \mu\text{m}\ .$$

An estimate for the total beam size at a distance d' from the monochromator, is:

$$\Delta y_{m1} = \sqrt{(\delta\theta_{ym1} \cdot d')^2 + \Delta y^2} \qquad (15)$$

$$\Delta x_{m1} = \sqrt{(\delta\theta_{xm1} \cdot d')^2 + \Delta x^2}\ . \qquad (16)$$

The beam flux is inversely proportional to the beam cross-sectional area A_o and A_{m1}. Thus, the ratio of the distorted to the undistorted beam fluxes is therefore:

$$\frac{F_{m1}}{F_o} = \frac{A_o}{A_{m1}} = \frac{\Delta x \cdot \Delta y}{\Delta x_{m1} \cdot \Delta y_{m1}}\ . \qquad (17)$$

Table IV compares the ratio of the distorted to the undistorted beam fluxes (F_{m1}/F_o) for the flat and inclined geometries using equation (17). The beam sizes are computed at a distance of 60 from the source. The monochromator is located at 30 m from the source. As before, the thermal strain data are based on reference [13]. Also, note that equation (17) does not take into account the particle source size.

From Table IV, we see that, although it is less severe than the brilliance loss, the flux loss is significant. For the worst case scenario presented here, the flux loss is by a factor of 1/0.21 = 4.8. Comparing flat and inclined crystals, we see that, as before, the effect of the fabrication-induced strain is worse for inclined crystals.

Finally, it should be pointed out that, despite the high losses of brilliance and flux of the beam from inclined crystals, the total throughput (total number of photons/s) from the inclined DCM should be about the same as that of the flat DCM. The rho-kick affects the horizontal divergence of the beam and is therefore a second order effect on θ. In other words, the rho-kicked reflected beam off the first crystal of the DCM will still be reflected from the second crystal because the change in $\theta 2_{inc}$ is very small.

V. SUMMARY

In summary, this paper presents simulations and supporting experimental measurements which indicate that small amounts of strains in the inclined crystal can cause a large increase in the horizontal reflected beam divergence. The "amplification factor" of the distortion can be as large as 19.7 for an 85° inclined crystal. With the current best estimates for fabrication- and thermal-induced strains, the beam brilliance loss may be as much as 100 times and the flux loss may be by as much as 4.8 times. Although the net throughput of the inclined DCM should be the same as the flat DCM, such severe losses in the beam brilliance and flux would appear to be unacceptable to most users.

In order to improve the performance of the inclined DCM, clearly, special attention must be given to minimizing the strains in the crystal. While it may be difficult to reduce the thermal-induced strains (for room-temperature-cooled crystals), there should be ways to reduce the fabrication-induced strains. Currently, most of the fabrication-induced strains originate from the bonding process. Thus, cooling geometries that do not require bonding, such as core-drilled crystals, may be more appropriate. In order to reduce the thermal-induced strains, it may be necessary to go to cryogenic cooling.

ACKNOWLEDGMENTS

This work was supported by the U.S. Department of Energy, BES-Materials Sciences, under Contract No. W-31-109-ENG-38.

[1]J. Hrdy, Rev. Sci. Instrum. 63, 459-460 (1992).
[2]A. Khounsary, Rev. Sci. Instrum. 63, 461-464 (1992).
[3]A. T. Macrander, D. R. Haeffner, and P. L. Cowan, Proc. SPIE 1740, 2-10 (1992).
[4]A. T. Macrander, W. K. Lee, R. K. Smither, D. M. Mills, C. S. Rogers, and A. M. Khounsary, Nucl. Instrum. Methods A319, 188-196 (1992).
[5]W. K. Lee, A. T. Macrander, D. M. Mills, C. S. Rogers, R. K. Smither, and L. E. Berman, Nucl. Instrum. Methods A320, 381-387 (1992).
[6]R. C. Blasdell and A. T. Macrander, Nucl. Instrum. Methods A347, 320-323 (1994).
[7]R. C. Blasdell, A. T. Macrander, and W. K. Lee, Nucl. Instrum. Methods A347, 327-330 (1994).
[8]W. H. Zachariasen, *Theory of X-Ray Diffraction in Crystals*, John Wiley & Sons, Inc., New York, 1945.
[9]R. W. James, *The Optical Principles of the Diffraction of X-Rays*, G. Bell and Sons, London, 1950.
[10]B. W. Batterman and H. Cole, Rev. Mod. Phys. 36, 681-717 (1964).
[11]P. P. Ewald, *P. P. Ewald and his Dynamical Theory of X-ray Diffraction*, edited by D. W. J. Cruickshank, H. J. Jeretschke, and N. Kato, International Union of Crystallography, Oxford University Press, 1992.
[12]R. J. Dejus, B. Lai, E. R. Moog, and E. Gluskin, Undulator A Characteristics and Specifications: Enhanced Capabilities, Argonne National Laboratory Report ANL/APS/TB-17 (1994).
[13]L. Assoufid, W.-K. Lee, and D. M. Mills, A Finite Element Analysis of Room Temperature Silicon Crystals for the APS Bending-Magnet and Insertion-Device Beams, Argonne National Laboratory Report ANL/APS/TB-19 (1994).

